Available online at www.sciencedirect.com
ScienceDirect
Trans. Nonferrous Met. Soc. China 30(2020) 1928−1942
Transactions of Nonferrous Metals Society of China
www.tnmsc.cn

Oxidation of chalcopyrite in air-equilibrated acidic solution: Inhibition with phenacyl derivatives

Paul CHIRIȚĂ[1], Mădălina I. DUINEA[1,2], Laura G. SÂRBU[3], Lucian M. BÎRSĂ[3], Mihaela BAIBARAC[4], Florinel SAVA[4], Elena MATEI[4]

1. Department of Chemistry, University of Craiova, Calea Bucuresti 107I, 200478, Craiova, Romania;
2. Department of Chemistry, Physics and Environment, "Dunarea de Jos" University of Galati, 111 Domneasca Street, Galati 800201, Romania;
3. Department of Chemistry, "Al. I. Cuza" University of Iasi, 11 Carol I Blv., Iasi 700506, Romania;
4. Lab. Optical Processes in Nanostructured Materials, National Institute of Materials Physics, P. O. Box MG-7, Bucharest, R077125, Romania

Received 2 November 2019; accepted 20 May 2020

Abstract: The effects of 4-(2-hydroxyphenyl)-2-(morpholin-4-yl)-1,3-thiazole (Pr02), 1-(3,5-dibromo-2-hydroxyphenyl)-1-oxoethan-2-yl-*N*,*N*-diethyldithiocarbamate (Pr04) and 1-(5-bromo-2-hydroxy-3-methylphenyl)-1-oxoethan-2-yl-*O*-ethyl xanthate (Pr06) on the aqueous oxidation of chalcopyrite ($CuFeS_2$) in air-equilibrated solution at a temperature of 25 °C and a pH of 2.5 were studied. The effects were investigated by using potentiodynamic polarization, electrochemical impedance spectroscopy (EIS), scanning electron microscopy coupled with energy dispersive X-ray (SEM/EDX) analysis, aqueous batch experiments, Fourier transform infrared (FTIR) spectroscopy, Raman scattering and quantum chemical calculations. It is found that the anodic current densities decrease in the order of EtOH > Pr02 > Pr04 > Pr06. These results, along with those of the EIS measurements, show that Pr02, Pr04 and Pr06 are effective anodic inhibitors of chalcopyrite aqueous oxidation. Both Raman scattering and FTIR spectroscopy indicate that the elemental sulfur, polysulfide and ferric oxyhydroxides that form on the surface of the mineral are not responsible when it comes to the aqueous oxidation inhibition of chalcopyrite. Quantum chemical calculations show that the adsorption of the tested compounds on the chalcopyrite surface is energetically favorable and so, it can explain the inhibiting effects that were observed.

Key words: chalcopyrite oxidation; phenacyl derivatives; inhibition; potentiodynamic polarization; quantum chemical calculation

1 Introduction

Chalcopyrite ($CuFeS_2$) is the most important copper-bearing mineral on the Terra. The aqueous oxidation of chalcopyrite existing in rocks or the waste resulting from the processing of ores causes the release of copper and other toxic elements present in its matrix (Pb, Cd, As, Sb, etc.) and the generation of acid drainage which seriously pollutes the natural waters [1,2]. Therefore, the aqueous oxidation of chalcopyrite has been extensively investigated [2−7]. In the environment, molecular oxygen (O_2) is a common oxidant [2]. The aqueous oxidation of chalcopyrite by O_2 can be summarized by the following overall reaction [8]:

$$CuFeS_2+4O_2=Cu^{2+}+Fe^{2+}+2SO_4^{2-} \quad (1)$$

Depending on the experimental conditions, chalcopyrite oxidation may be partial, with the sulfur from $CuFeS_2$ being oxidized to elemental sulfur [5,8,9]:

Corresponding author: Paul CHIRIȚĂ; Tel/Fax: +40-251597048; E-mail: paulxchirita@gmail.com
DOI: 10.1016/S1003-6326(20)65351-1

$$CuFeS_2+4H^++O_2=Cu^{2+}+Fe^{2+}+2S+2H_2O \quad (2)$$

Elemental sulfur (S^0) can be found embedded in polysulfide species ($^-S-S^0_n-S^-$) [10−13]. Together with iron oxyhydroxides (resulted from the hydrolysis of Fe^{3+}, the product of Fe^{2+} oxidation [9,14]), the elemental sulfur and polysulfide species form a surface layer (SL) which is considered the main factor that inhibits the aqueous oxidation of chalcopyrite [4,7,15,16]. One considers that the inhibition represents an important problem for the optimal copper extraction by atmospheric leaching process [4]. Yet, the low rate of aqueous oxidation of chalcopyrite could be the result of the reaction complexity (it is a multi-step reaction). Those up to 16 electrons lost by chalcopyrite can only be transferred in a sequence of several elementary reactions, the number of electrons transferred in each elementary reaction being no more than two [17,18].

In contrast, the SL formed on chalcopyrite does not sufficiently slow its natural dissolution [5]. Hence, chalcopyrite is seen as an important contributor to acid metalliferous drainage [2], a major environmental problem. Considering the results obtained for other sulfides [19−21], a way to inhibit the chalcopyrite aqueous oxidation could be the treatment of the mineral with various organic compounds. According to the general mechanism of metal corrosion [22−26], the adsorbed organic molecules obstruct the transfer of electrons to the oxidant. As with metals and other metal sulfides, the heteroatoms and multiple bonds in the structure of the organic molecules facilitate their adsorption on the chalcopyrite surface, fact that blocks the active centers of the mineral surface.

The aim of this study is to examine the influence of three phenacyl derivatives (4-(2-hydroxyphenyl)-2-(morpholin-4-yl)-1,3-thiazole (Pr02), 1-(3,5-dibromo-2-hydroxyphenyl)-1-oxoethan-2-yl-*N,N*-diethyldithiocarbamate (Pr04) and 1-(5-bromo-2-hydroxy-3-methylphenyl)-1-oxoethan-2-yl-*O*-ethyl xanthate (Pr06)) on the aqueous oxidation of chalcopyrite in air-equilibrated acidic solution. The heteroatoms (O, S, N, Br) and double bonds present in their structures suggest that the three compounds can be adsorbed on the chalcopyrite surface, for example, they are adsorbed on the sphalerite surface [20]. The effects of organic molecules on chalcopyrite reactivity were investigated through potentiodynamic polarization, electrochemical impedance spectroscopy (EIS) and aqueous batch experiments. The uninhibited/inhibited surfaces were characterized through scanning electron microscopy coupled with energy dispersive X-ray (SEM/EDX) analysis, Raman scattering and Fourier transform infrared (FTIR) spectroscopy. The relationship between the tested structures and their inhibitory effect was studied by quantum chemical method.

2 Experimental

2.1 Materials

A natural $CuFeS_2$ sample was used in the present study. X-ray diffraction (XRD) analysis (Fig. 1) was carried out using a Bruker A8 Advanced diffractometer provided with Cu target tube and Lynx Eye detector. The X-ray diffraction diagrams were recorded in the 2θ range of 5°−80° with the angular step 0.02° and measuring time per angular position: 142 s. A major body-centered tetragonal $CuFeS_2$ phase was identified in the Fig. 1. In this sample there is a hexagonal SiO_2 phase. Also a minor phase ($(Zn,Al,Cu)_3(Si,Al)_2O_5$-$(OH)_4$-base-centered orthorhombic) is present in the sample. No pyrite phase is detected by XRD analysis. The presence of pyrite is important because it can increase the rate of chalcopyrite oxidation, the maximal effect was observed for a pyrite-to-chalcopyrite particle loading ratios in excess of 4 [27]. The impurities determined by ICP-OES method are: Mn (38.0 mg/kg), Co (19.7 mg/kg), Ni (39.8 mg/kg), Zn (195.2 mg/kg), As (182.5 mg/kg), Ag (7.7 mg/kg), Cd (1.1 mg/kg), Sb (34.2 mg/kg) and Pb (197.9 mg/kg).

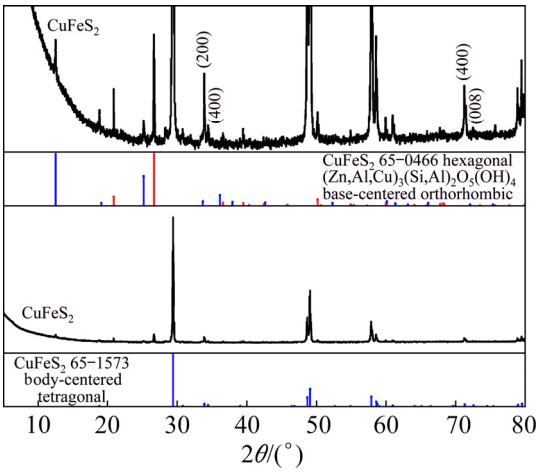

Fig. 1 XRD patterns of $CuFeS_2$ powder

The acid solutions were prepared from reagent grade purity HCl. Distilled water was used for the preparation of acid solutions with initial pH 2.50.

The molecular structures of the three tested compounds are shown in Fig. 2. These compounds were synthesized as previously described [20].

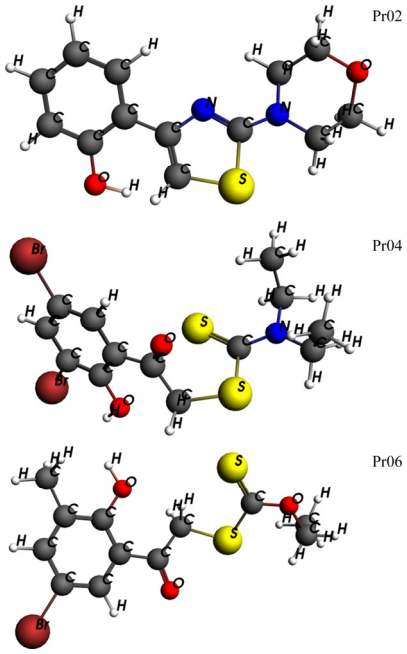

Fig. 2 Structures of Pr02, Pr04 and Pr06 (Local density approximation was used for the optimization)

2.2 Working electrodes

The working electrodes, of type carbon paste electrodes (CPE), were prepared according to a procedure used by CHIRITA et al [20]. The natural $CuFeS_2$ sample was ground under ethyl alcohol, dried and sieved. The particle fraction with diameter less than 125 μm was divided into four. One part was dipped in pure ethanol for 4 h, while the other three parts were dipped in 1 mmol/L ethanolic solutions of the tested compounds for the same amount of time. Each treated solid sample was then filtered and dried under vacuum in a desiccator. An isolated Cu wire (isolation prevents the contact between the metal and the solution) with a diameter of 4 mm was immersed in a graphite−paraffin wax mixture (2.0 g and 2.4 g, respectively) and heated at 75 °C. 0.02 g of each chalcopyrite sample treated as mentioned above was placed in a Teflon mould with 5 mm in diameter and the extremity of the copper wire covered with the hot mixture of graphite−paraffin wax was instantly pressed on the $CuFeS_2$ particles in the mould. The resulting hemisphere composed from the mixture of graphite−paraffin wax and covered by a $CuFeS_2$ bed is 5 mm in diameter.

2.3 Electrochemistry

Electrochemical experiments were performed in a three-electrode cell consisting of a working electrode (CPE), a saturated calomel electrode (SCE) as reference electrode, and a platinum counter electrode. Potentiodynamic polarization data were recorded using a ZAHNER ZENNIUM electrochemical workstation, at a scan rate of 0.001 V/s in the potential range from −0.250 to 0.250 V vs open circuit potential (OCP). The recorded potential values were reported to the standard hydrogen electrode (SHE) potential. EIS measurements were performed in a frequency range from 100 kHz to 10 mHz with amplitude of 0.010 V using AC signals at OCP.

2.4 Aqueous batch experiments

Aqueous batch experiments were performed in Erlenmeyer flasks in contact with atmosphere, at a temperature of 25 °C. The temperature was maintained constant with a thermostated bath. The flasks were filled with 0.25 L of the air-equilibrated HCl solution with initial pH 2.50 and were homogenized by slow bubbling of air. At the start of the experiments, 0.5 g $CuFeS_2$ was suspended in the air-equilibrated HCl solution. Each experiment lasted for 63 days. Periodically, aliquots of the solution were extracted from the reaction system through a 0.2 μm filter and analyzed for total dissolved iron. The dissolved ferric iron was reduced by a solution of 10% hydroxylamine, after which the concentration of the total dissolved iron was determined through spectrophotometry (PG Instruments T70-UV−Vis spectrophotometer) using the 2,2'-dipyridyl method at 522 nm. At the end of the experiments, 25 mL of solution was collected with a syringe connected to a 0.2 μm filter. The resulting solutions were analyzed for dissolved SO_4^{2-} by turbidimetry using the $BaSO_4$ method at 420 nm [28].

2.5 FTIR spectroscopy

The FTIR spectra of $CuFeS_2$ samples were recorded with a Bruker Alpha spectrometer using KBr technique. The spectral range was between 375 and 4000 cm^{-1} and the resolution was 4 cm^{-1}. The

FTIR measurements were performed soon after pellet preparation, in order to avoid the oxidation of the chalcopyrite particles.

2.6 SEM and EDX analysis

A Zeiss EVO 50 XVP scanning electron microscope (SEM) equipped with an energy dispersive X-ray spectroscopy (EDX) Quantax Bruker 200 system as attachment was used to investigate the morphology and surface composition of the $CuFeS_2$ samples.

2.7 Raman spectroscopy

A T64000 Raman spectrophotometer, acquired from Horiba Jobin Yvon, endowed with Ar laser was used at recording of the Raman spectra of treated $CuFeS_2$. The Raman resolution was 2 cm^{-1}.

2.8 Quantum chemistry analysis

For the estimation of the electronic properties of chalcopyrite surface, phenacyl derivatives (PD) and $CuFeS_2$-PD complexes, the Amsterdam Density Functional (ADF, 2016 program version) was used [29,30]. Scalar relativistic effects were taken into account using the zero order regular approximation (ZORA) [31−33].

As with sphalerite [20], for the modeling of the chalcopyrite(110) surface, a cluster of 4 atoms was used. It is derived from the optimized (110) surface of chalcopyrite and has the stoichiometry $CuFeS_2$ (Fig. 3).

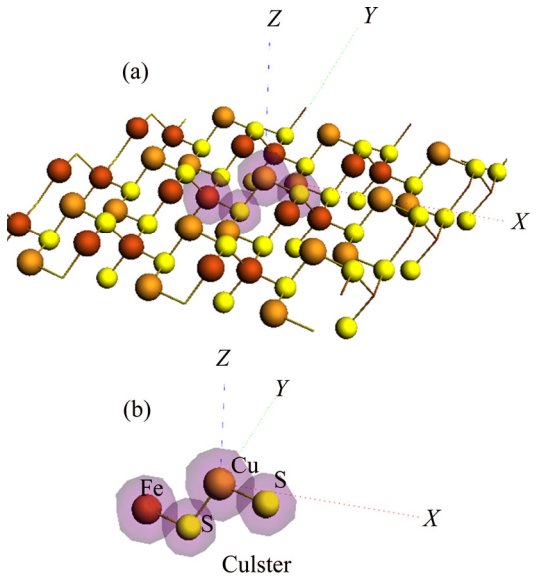

Fig. 3 Chalcopyrite(110) surface (a) and derived $CuFeS_2$ cluster (b) used to model adsorption of three tested derivatives (Pr02, Pr04 and Pr06)

The local density approximation (LDA) was used to optimize the chalcopyrite geometry [34]. Double-zeta Slater type orbital basis set with a large frozen core was used to characterize the atomic electron configuration of chalcopyrite(110) surface. The geometry of isolated phenacyl derivatives was optimized using, on one hand, the exchange correlation functional GGA-PW91 [20,35] and on the other hand, local density approximation (LDA). Double-zeta quality basis set with a large frozen core was used to characterize the atomic electron configuration of phenacyl derivatives. Density functional theory (DFT) calculations for $CuFeS_2$-PD complexes were performed using LDA, the double-zeta quality basis set and large frozen core. Adsorption of PD molecules has been set on either Cu or Fe atoms (Fig. 3). The default program settings have been used as convergence criteria for all calculations.

The adsorption energy (E_{ad}) is computed using the following relationship:

$$E_{ad}=E_{CuFeS_2\text{-}PD}-E_{PD}-E_{CuFeS_2} \quad (3)$$

where E_{CuFeS_2} is the bond energy of $CuFeS_2$ cluster, E_{PD} is the bond energy of phenacyl derivative, and $E_{CuFeS_2\text{-}PD}$ is the bond energy of the $CuFeS_2$-PD complex.

A negative adsorption energy (E_{ad}) indicates a stabilization of the $CuFeS_2$-PD complex with respect to the $CuFeS_2$ cluster and phenacyl derivative. Bond energies of $CuFeS_2$-PD complex, $CuFeS_2$ cluster and phenacyl derivatives are computed as a difference between the energy of the corresponding species and its constituent atoms [30].

3 Results and discussion

3.1 Polarization measurements

The polarization curves of $CuFeS_2$ electrodes dipped in air-equilibrated acidic solutions (initial pH 2.50 and 25 °C) are shown in Fig. 4.

The oxidation potential, φ_{ox}, varies slightly when chalcopyrite was treated with pure ethanol (0.385 V) and solutions of Pr02 (0.412 V) and Pr06 (0.433 V) in ethanol. φ_{ox} is clearly shifted in cathodic direction when the $CuFeS_2$ was treated with ethanolic solution of Pr04 (0.217 V). The cathodic current densities (J) of chalcopyrite treated with the three organic compounds fluctuate around

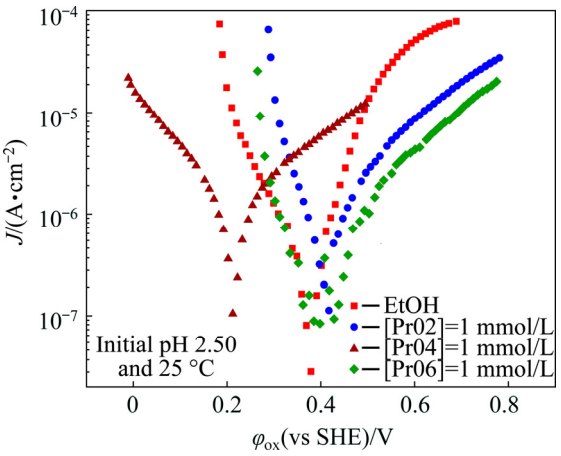

Fig. 4 Potentiodynamic polarization curves for chalcopyrite electrodes treated with EtOH (pure ethanol) and 1 mmol/L solutions of Pr02, Pr04 and Pr06 in ethanol

the cathodic current densities recorded for the chalcopyrite treated with pure ethanol. The anodic current densities decrease when the $CuFeS_2$ is treated with ethanolic solutions of the tested derivatives. The anodic J values decrease as follows: EtOH > Pr02 > Pr04 > Pr06. Since the current densities and inhibitory effect can be correlated [20] (i.e., as the current densities of the samples treated with phenacyl derivatives are lower than those of the sample treated with pure ethanol, the more pronounced the inhibitory effect), it results that all the three tested compounds (Pr02, Pr04 and Pr06) are effective anodic inhibitors of the aqueous oxidation of chalcopyrite.

3.2 EIS measurements

EIS measurements were performed for the identification and characterization of the physical and chemical processes which occur at the electrode−solution interface. EIS spectra in the form of Nyquist plots are presented in Fig. 5.

The shape of the Nyquist curves obtained for chalcopyrite treated with EtOH and the solutions of Pr02 and Pr06 in ethanol is very similar. These impedance spectra exhibit an incomplete capacitive loop. It can be mainly assigned to charge transfer resistance at the electrode−solution interface [36,37]. The Nyquist curve obtained for the chalcopyrite treated with ethanolic solution of Pr04 is different. It exhibits two capacitive loops. The low frequency capacitive loop can be assigned to charge transfer resistance, whilst the high frequency capacitive loop can be assigned to a SL formed on the surface of the mineral during its oxidation [21,37]. The experimental results suggest that the aqueous oxidation of chalcopyrite treated with pure ethanol (EtOH) and the solutions of Pr02 and Pr06 in ethanol is controlled by a surface chemical reaction, and, respectively, the oxidation of chalcopyrite treated with Pr04 is controlled both by a surface chemical reaction and the diffusion of the reactants and/or reaction products across the SL formed on the surface of the mineral (the corresponding capacitive loop becomes evident) [21,37,38].

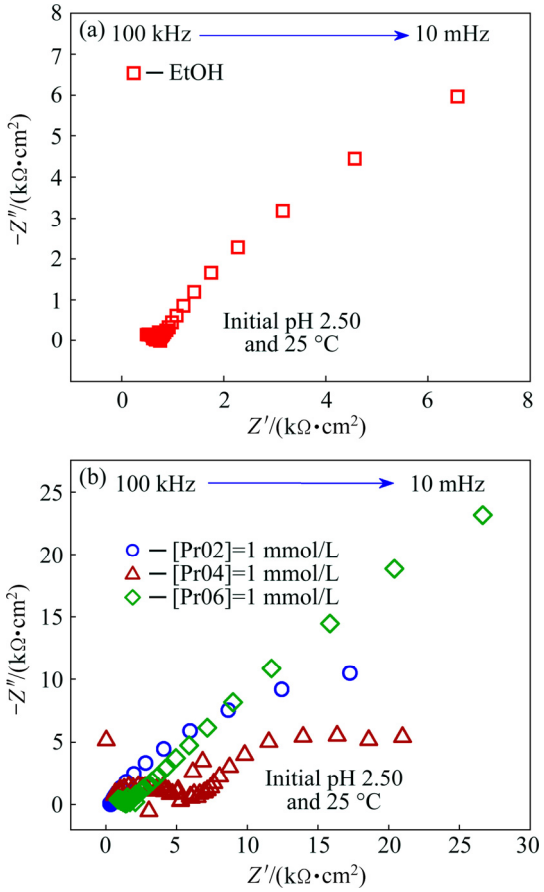

Fig. 5 Nyquist impedance spectra of chalcopyrite electrodes treated with EtOH (a) and 1 mmol/L solutions of Pr02, Pr04 and Pr06 in ethanol (b) (To avoid any ambiguity produced by the data points superimposition, the impedance spectrum of chalcopyrite electrode treated with EtOH (Fig. 5(a)) is separately presented)

Taking into account that the charge transfer resistance is directly proportional to the extension of the Nyquist curve along the x-axis to low frequencies [24], it results that the charge transfer resistance (which is inversely proportional to the current density) of the chalcopyrite treated with

EtOH (Fig. 5(a)) is lower than that of the chalcopyrite treated with solutions of Pr02, Pr04 and Pr06 in ethanol (Fig. 5(b)). This finding is in good agreement with the results of polarization measurements, which indicates that the anodic current densities decrease (i.e., charge transfer resistances increase) when the chalcopyrite particles are treated with ethanolic solutions of the three tested compounds.

3.3 Aqueous batch experiments

Figure 6(a) shows the variation of the concentration of total dissolved iron ([Fe_{tot}]). For the all chalcopyrite samples, [Fe_{tot}] increases during the first 5−6 days of contact between mineral and air-equilibrated acidic solutions.

The highest [Fe_{tot}] was observed for the chalcopyrite treated with pure ethanol ([Fe_{tot}]= 340 μmol/L) and was followed by chalcopyrite treated with Pr04 ([Fe_{tot}]=328 μmol/L), Pr06 ([Fe_{tot}]=285 μmol/L) and, respectively, Pr02 ([Fe_{tot}]=255 μmol/L). After approximately 7 days of contact between chalcopyrite samples and air-equilibrated acidic solutions, [Fe_{tot}] decreases by 2−3 times and remains lower than 150 μmol/L until the experiments end. The fact that after 7 days of chalcopyrite oxidation the pH is higher than 2.5 (Fig. 6(b)) indicates that the decrease of [Fe_{tot}] is due to the ferric iron precipitation [14,39]. As a general trend, the potential φ(vs SHE) decreases during the interaction of chalcopyrite samples with the acidic solutions (Fig. 6(c)). Most likely, the decrease is caused by the oxygen consumption by the surface iron and sulfur. The most important decrease of φ is observed for the chalcopyrite sample treated with pure ethanol. This finding indicates that this chalcopyrite sample consumes the most amount of oxygen (i.e., undergoes the highest degree of oxidation). A comparison between [Fe_{tot}] and [SO_4^{2-}] registered at the moment the experiments ended (i.e., after 63 days) is presented in Fig. 7.

In all the cases, [Fe_{tot}]>[SO_4^{2-}]. Moreover, for the chalcopyrite sample treated with pure ethanol, [SO_4^{2-}]=0 mol/L. These findings indicate that for this particular sample, the surface sulfur is either entirely oxidized to polysulfide and/or elemental sulfur [40−43] or lost as gaseous H_2S [43], or the formed sulfate is adsorbed on the precipitated ferric oxyhydroxides. The large initial variations observed for [Fe_{tot}] and the absence of dissolved SO_4^{2-} at the end of the experiment performed with chalcopyrite treated with pure ethanol indicate that both dissolved iron and sulfate are not adequate

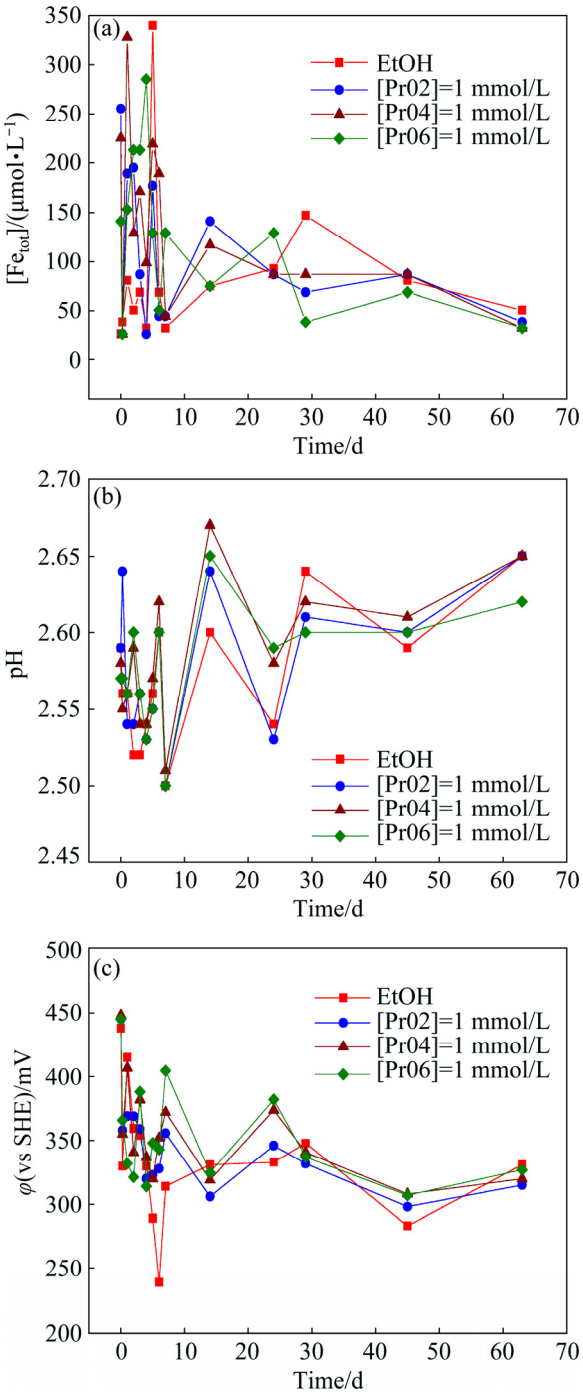

Fig. 6 Evolution of [Fe_{tot}] (a), pH (b) and φ (c) as function of time for uninhibited (treated with EtOH) and inhibited (treated with 1 mmol/L solutions of Pr02, Pr04 and Pr06 in ethanol) chalcopyrite particles reacted at 25 °C and pH (before immersion of chalcopyrite) of 2.50

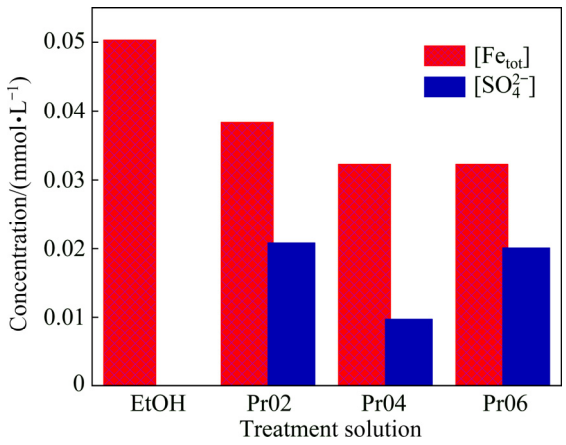

Fig. 7 $[Fe_{tot}]$ and $[SO_4^{2-}]$ measured at moment aqueous batch experiments ended

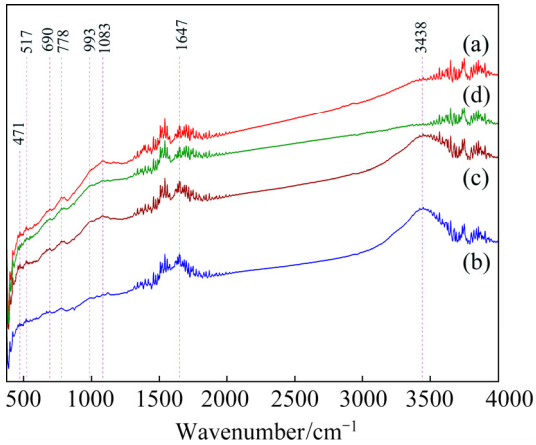

Fig. 8 FTIR spectra of $CuFeS_2$ particles dipped in EtOH (a) and 1 mmol/L solutions of Pr02 (b), Pr04 (c) and Pr06 (d) in ethanol

progress variables for the aqueous oxidation of $CuFeS_2$ at pH 2.5. For example, a part of dissolved H_2S can be converted to gaseous H_2S and consequently less SO_4^{2-} forms during $CuFeS_2$ aqueous oxidation, and the reaction rate is thus underestimated. In addition, the copper is a species that does not participate in the electrons transfer between chalcopyrite and dissolved oxygen, and, consequently, it can be a reliable progress variable only for the non-oxidative dissolution of chalcopyrite. Hence, the progress variable that best describe the kinetics of chalcopyrite oxidative dissolution is the amount of transferred electrons, which can be evaluated from polarization measurements.

3.4 FTIR measurements

FTIR analysis offers information about the nature of phases present in the $CuFeS_2$ samples at the ending of the treatment with EtOH and 1 mmol/L solutions of the organic compounds (Fig. 8).

The bands up to 1100 cm^{-1} can be ascribed to elemental sulfur, disulfide and polysulfide (471 cm^{-1}); amorphous iron oxides (517 cm^{-1}); FeOOH phases or amorphous $Fe(OH)_3$ (690 and 778 cm^{-1}); sulfite, thiosulfate, sulfate and sulfate bonds to protons and/or metal cations (993 and 1083 cm^{-1}) [14,36,40,44−46]. The bands situated at high wavenumbers (>1100 cm^{-1}) can be attributed to H—O—H deformation (1647 cm^{-1}) [46,47] and goethite or amorphous $Fe(OH)_3$ (3438 cm^{-1}) [14,36,40]. The signals around 1500 cm^{-1} are specific of carbonate species [14]. From Fig. 8 one can observe that the bands centered at 3438 cm^{-1} present in the spectra of $CuFeS_2$ treated with solutions of Pr02 and Pr04 in ethanol are missing in the spectra of $CuFeS_2$ treated only with ethanol and ethanolic solution of Pr06. According to the results by TAO et al [48], the hydrophobicity of the $CuFeS_2$ samples treated only with ethanol and ethanolic solution of Pr06 indicates the presence of elemental sulfur and polysulfide species on their surfaces. The fact that both the surface of $CuFeS_2$ treated with pure ethanol and the surface of chalcopyrite treated with ethanolic solution of Pr06 contain ferric oxyhydroxides, polysulphide and elemental sulfur and their reactivity is different indicates that these species do not affect aqueous oxidation of chalcopyrite. Accordingly, it is reasonable to assume that the observed inhibitory effect is caused by the adsorption of the three tested derivatives on the mineral surface. Yet, the polarization and EIS data indicate that the SL has some influence on the mechanism of oxidation of chalcopyrite treated with Pr04 (the overall reaction is under mixed control, surface reaction and diffusion), without the inhibitory effect being absent. Thus, even if not totally, the adsorption of the Pr04 on the chalcopyrite surface still obstructs its aqueous oxidation.

3.5 Raman spectroscopy

According to Fig. 9, the main Raman lines of $CuFeS_2$ are situated in the ranges of 100−300, 400−600 and 1200−1400 cm^{-1}, these being peaked at 212−272, 363, 473, 572 and 1280 cm^{-1}.

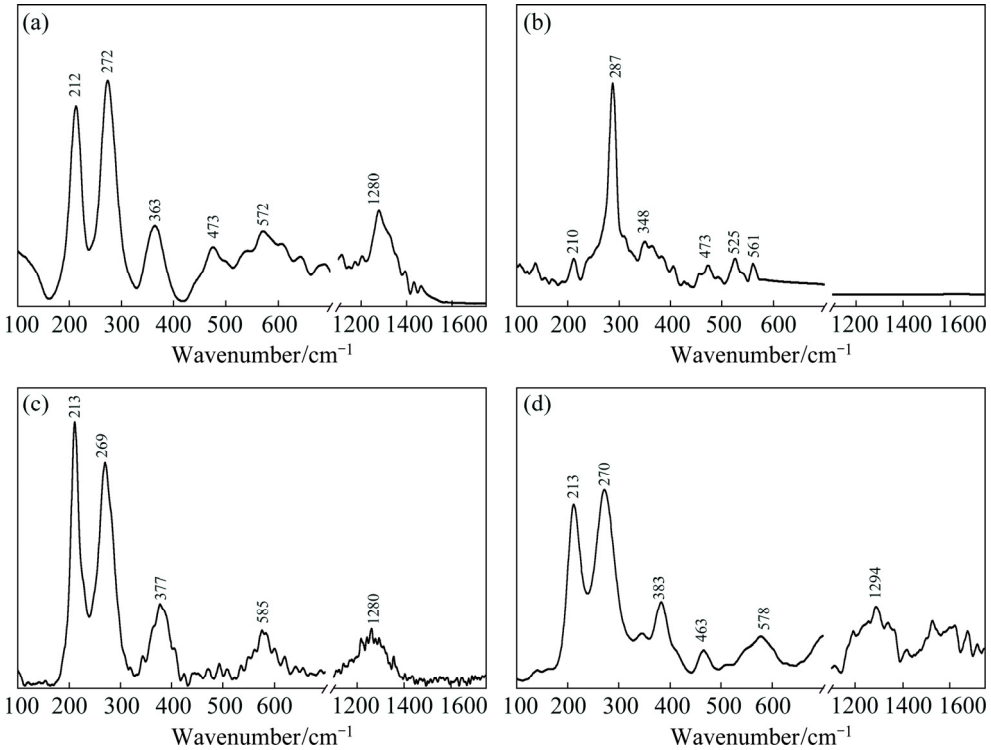

Fig. 9 Raman spectra of $CuFeS_2$ immersed in EtOH (a) and 1 mmol/L ethanolic solutions of Pr02 (b), Pr04 (c) and Pr06 (d), respectively

The first three Raman lines are assigned to the A_1, B_2 and E modes [49,50]. Raman lines localized in the 500−700 and 1200−1400 cm^{-1} ranges are assigned to the S—O and SO_4 bending vibrational modes [51]. The Raman spectra of $CuFeS_2$ are not changed in the presence of Pr04 and Pr06. In the presence of Pr02, the following changes are observed to be induced to the $CuFeS_2$ Raman spectrum: 1) a decreasing in the relative intensity of the Raman line peaked at 212 cm^{-1}; 2) an up-shift of the Raman line from 272 to 287 cm^{-1}; 3) a down-shift of the Raman line from 363 to 348 cm^{-1} and 4) the disappearance of the Raman line found in the 1200−1400 cm^{-1} range. In our opinion, these changes must to be correlated with the crystal lattice orientation and the presence of defects and/or impurities [52] induced by the chemical adsorption of Pr02 onto the $CuFeS_2$ surface.

3.6 SEM and EDX analysis

Chalcopyrite particles of the four samples used to make the carbon paste electrodes were also investigated by SEM and EDX analyses.

The SEM images of chalcopyrite samples are displayed in Fig. 10. Their surface shows a similar morphology. The particles are rough solids with multiple sharp corners and edges which are produced during the grinding. The EDX data (Fig. 11) show that copper, iron and sulfur mainly compose the surface of particles.

3.7 Quantum chemical modeling of adsorption of PDs on chalcopyrite

The quantum chemical parameters of the isolated phenacyl derivatives (energy of the lowest unoccupied molecular orbital (E_{LUMO}), energy of the highest occupied molecular orbital (E_{HOMO}), energy band gap ($\Delta E=E_{LUMO}-E_{HOMO}$) and dipole moment ($\mu$)) were computed with LDA and GGA-PW91, respectively [20]. The frontier molecular orbital electron densities evaluated by LDA are presented in Fig. 12.

These frontier molecular orbital electron densities are very similar with those computed with exchange correlation GGA-PW91 [20]. For Pr04 and Pr06, the central heteroatoms participate in electron donation (HOMO of phenacyl derivatives in Figs. 12(c, e)), whereas the aromatic moiety is mostly participated for accepting electrons (LUMO of phenacyl derivatives in Figs. 12(d, f)). As far as Pr02 is concerned, all the central heteroatoms (O, N and S), as well as the aromatic rings are responsible

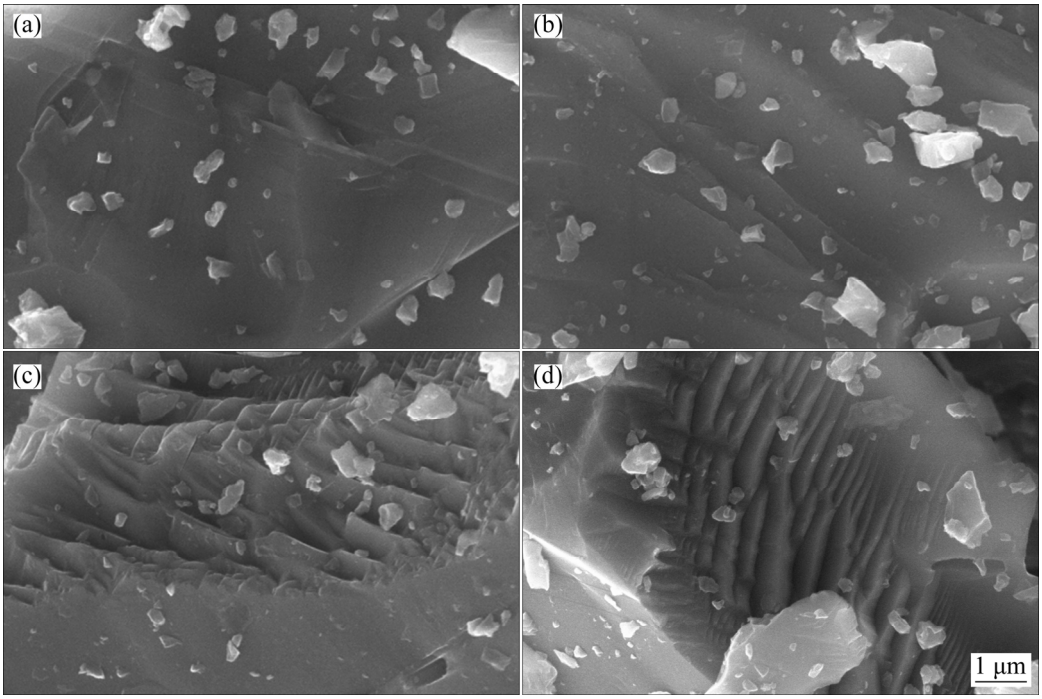

Fig. 10 SEM images of $CuFeS_2$ immersed in EtOH (a) and 1 mmol/L ethanolic solutions of Pr02 (b), Pr04 (c) and Pr06 (d)

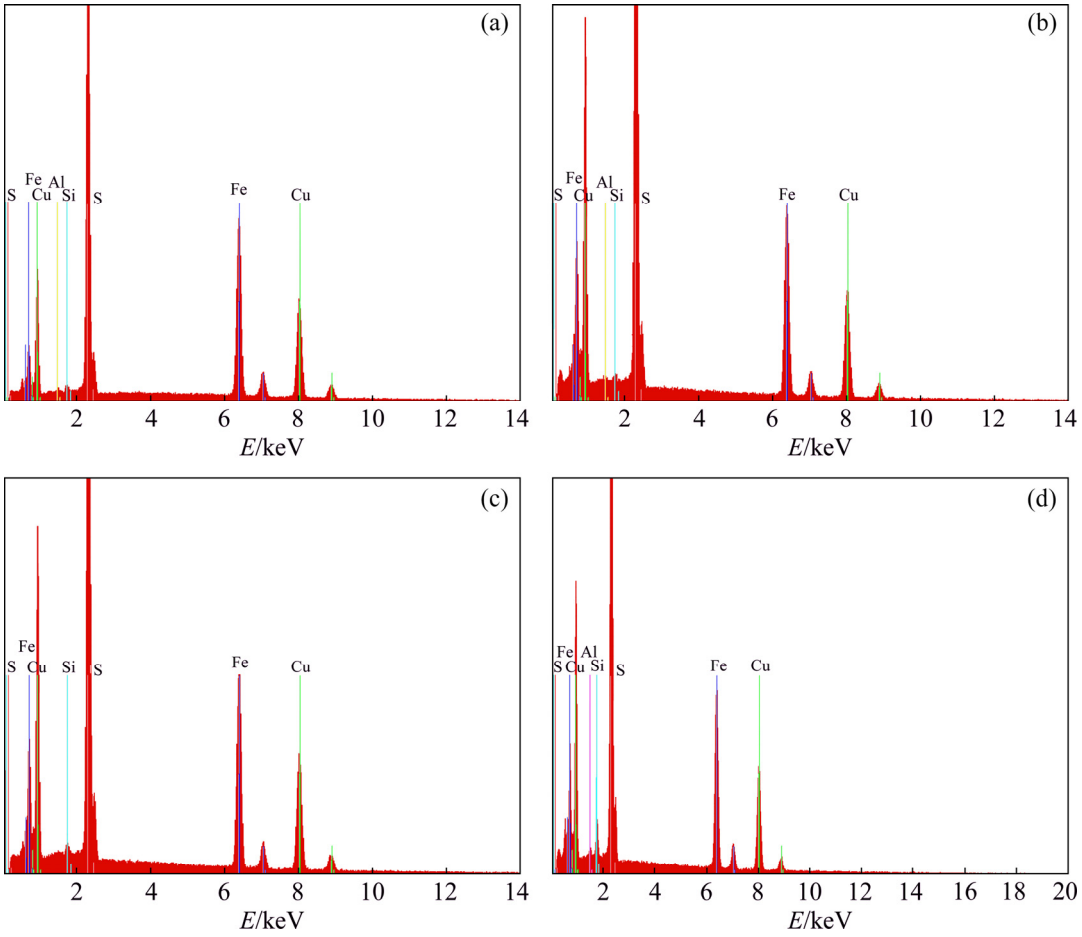

Fig. 11 EDX analyses of $CuFeS_2$ immersed in EtOH (a) and 1 mmol/L ethanolic solutions of Pr02 (b), Pr04 (c) and Pr06 (d)

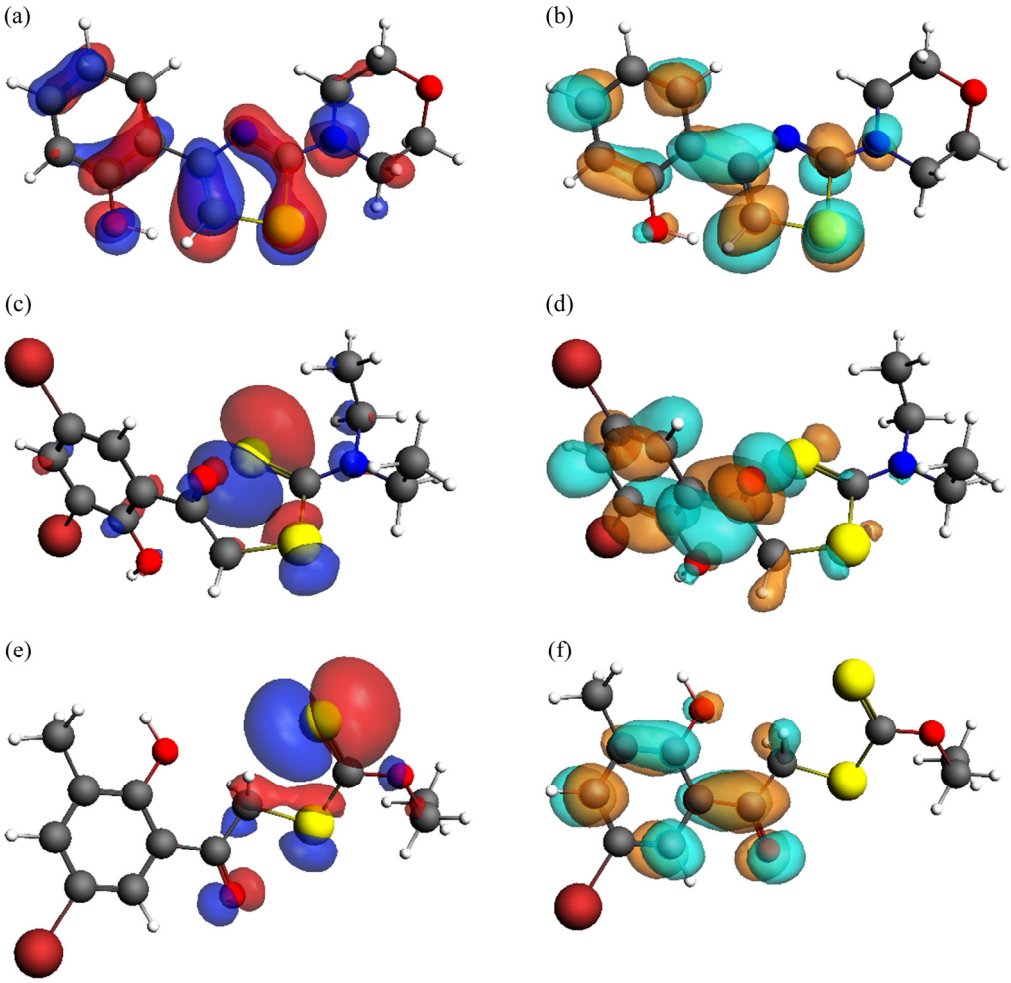

Fig. 12 HOMO (a, c, e) and LUMO (b, d, f) orbital density distribution of three tested compounds: (a, b) Pr02; (c, d) Pr04; (e, f) Pr06 (The orbital distributions were evaluated by LDA. The orbital distributions evaluated by GGA-PW91 can be found in Ref. [20])

for the donation and acceptance of electrons (HOMO and LUMO of phenacyl derivative in Figs. 12(a, b)). Table 1 presents the quantum chemical parameters (energy of the lowest unoccupied molecular orbital; energy of the highest occupied molecular orbital; energy band gap and dipole moment) evaluated for the three phenacyl derivatives.

Adsorption of phenacyl derivatives was evaluated on both Fe and Cu atoms of the $CuFeS_2$ cluster (Fig. 13). Both Fe and Cu atoms can be terminal atoms of the irregular regions (edges and corners) of the chalcopyrite surface (Fig. 10). Such atoms, with unsatisfied valences, are very active centers that will quickly react. Consequently, blocking them, for example by adsorption, is essential to stopping the oxidation reaction of the chalcopyrite. As with sphalerite [20], it was studied the scenario in which the tested derivatives are adsorbed to $CuFeS_2$ cluster by the means of sp^3 hybridized sulfur. This kind of sulfur appears in all phenacyl derivatives and therefore the comparison of the obtained results offers relevant information regarding the effect of the three organic compounds on the aqueous oxidation of chalcopyrite. The

Table 1 Quantum chemical parameters for Pr02, Pr04 and Pr06 in gas phase (The parameters are evaluated by LDA. The quantum chemical parameters evaluated by GGA-PW91 can be found in Ref. [20])

Phenacyl derivate	ΔE/ (kJ·mol^{-1})	E_{HOMO}/ (kJ·mol^{-1})	E_{LUMO}/ (kJ·mol^{-1})	μ/ Debye
Pr02	309.8	−546.1	−236.3	3.301
Pr04	231	−554	−322.9	4.349
Pr06	220.5	−564.5	−343.9	4.071

adsorption energies (E_{ad}) are presented in Table 2. From Table 2 we can see that, E_{ad}<0 kJ/mol, either that bond energies of phenacyl derivatives (E_{PD}) were computed with LDA or GGA-PW91, respectively. These results suggest that the adsorption of the tested derivatives on Fe and Cu atoms is energetically favorable. When the bond energies of three PDs are computed with LDA, the most stable structure is Pr06 adsorption on Fe atom and the most unstable is Pr02 adsorption on Cu atom. If the bond energy of phenacyl derivatives is estimated with GGA-PW91, the most stable structure is Pr04 adsorption on Fe atom and the most unstable is Pr06 adsorption on Cu atom. The bond lengths presented in Fig. 13 are: 2.320 Å (S(PD)—Cu(cluster)); 2.363 Å (Cu—S bond in the $CuFeS_2$ cluster); 2.300 Å (S(PD)—Fe(cluster)); and 2.201 Å (Fe—S bond in the $CuFeS_2$ cluster).

Although there could be many other stable structures than those shown in Fig. 13, the negative

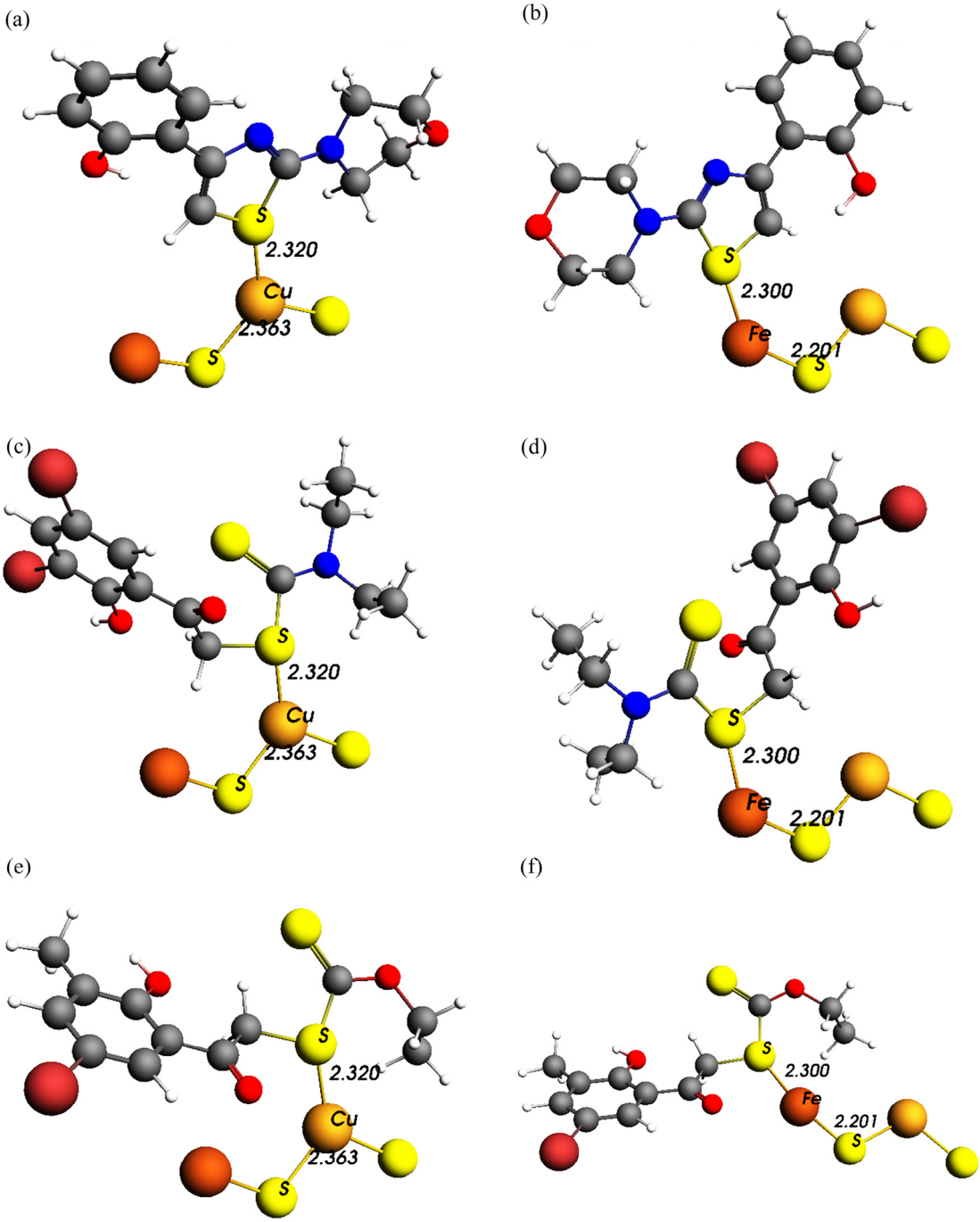

Fig. 13 Geometries of adsorption structures of Pr02 (a, b), Pr04 (c, d) and Pr06 (e, f) on $CuFeS_2$ cluster derived from chalcopyrite(110) surface (The adsorption was realized on Cu (a, c, e) or Fe (b, d, f) atoms. Distances are given in Å)

Table 2 Adsorption energies (E_{ad}) for Pr02, Pr04 and Pr06 on Cu and Fe atoms of $CuFeS_2$ cluster derived from chalcopyrite(110) surface

Chalcopyrite/PD optimizations	Center of adsorption	E_{ad}/(kJ·mol^{-1})		
		$CuFeS_2$-Pr02	$CuFeS_2$-Pr04	$CuFeS_2$-Pr06
LDA/LDA	Fe	−89.3	−102.4	−133.9
	Cu	−65.6	−78.8	−115.5
LDA/GGA	Fe	−1465.0	−1507.0	−1378.4
	Cu	−1441.4	−1483.4	−1360.0

values obtained for E_{ad} are enough to reveal the importance of the PDs adsorption on the chalcopyrite surface in the control of its aqueous oxidation. It is considered that the inhibitory effect of organic compounds increases when μ increases, and E_{ad} and ΔE decrease [22−26,53−55]. Starting from these considerations, the anodic current densities are well correlated with E_{ad} values evaluated by LDA/LDA optimization and ΔE values. Instead, the E_{ad} values evaluated by LDA/GGA optimization and μ underestimate the inhibitory effect of Pr06 on the aqueous oxidation of chalcopyrite.

4 Conclusions

(1) Pr02, Pr04 and Pr06 inhibit the aqueous oxidation of chalcopyrite. The three organic derivatives act as anodic inhibitors. The values of the anodic current densities of the chalcopyrite electrodes treated with pure ethyl alcohol and ethanolic solutions of the three phenacyl derivatives decrease in the following order of EtOH > Pr02 > Pr04 > Pr06. These findings are supported by the results of impedance and aqueous batch experiments.

(2) Both polarization and impedance data show that the electrochemical behavior of $CuFeS_2$ sample treated with ethanolic solution of Pr04 is different from that of the other chalcopyrite samples. The aqueous oxidation of chalcopyrite treated with EtOH and the solutions of Pr02 and Pr06 in ethanol is controlled by a surface reaction, while the oxidation of chalcopyrite treated with Pr04 is controlled by a mixed regime of a surface reaction and diffusion.

(3) Raman scattering and FTIR spectroscopy indicate that elemental sulfur, polysulfide and ferric oxyhydroxides are not responsible for the inhibition of the aqueous oxidation of chalcopyrite.

(4) Theoretical calculations show that the adsorption of the three tested derivatives on chalcopyrite is energetically favorable (E_{ad}< 0 kJ/mol). Hence, it is reasonable to assume that the adsorbed phenacyl derivatives obstruct the aqueous oxidation of $CuFeS_2$.

(5) Our findings show that aqueous oxidation of $CuFeS_2$ is rather controlled by the adsorbed organic matter than the SL formed on its surface. Most likely, the adsorbed organic molecules interpose between chalcopyrite and the dissolved oxygen and do not allow the transfer of electrons from mineral to oxidant. Future investigations should be planned to evaluate the effects of other organic molecules on the aqueous oxidation of chalcopyrite to find the organic structure that most efficiently controls the reaction.

Acknowledgments

This work was partly supported by a grant of the Romanian National Authority for Scientific Research, CNDI−UEFISCDI, project number 51/2012.

References

[1] HU J, TIAN G, ZI F, HU X. Leaching of chalcopyrite with hydrogen peroxide in 1-hexyl-3-methyl-imidazolium hydrogen sulfate ionic liquid aqueous solution [J]. Hydrometallurgy, 2017, 169: 1−8.

[2] KIMBALL B E, RIMSTIDT J D, BRANTLEY S L. Chalcopyrite dissolution rate laws [J]. Applied Geochemistry, 2010, 25: 972−983.

[3] VELASQUEZ P, LEINEN D, PASCUAL J, RAMOS-BARRADO J R, GREZ P, GOMEZ H, SCHREBLER R, DEL R, CORDOVA R. A chemical, morphological, and electrochemical (XPS, SEM/EDX, CV, and EIS) analysis of

electrochemically modified electrode surfaces of natural chalcopyrite ($CuFeS_2$, and pyrite (FeS_2, in alkaline solutions [J]. The Journal of Physical Chemistry B, 2005, 109: 4977−4988.

[4] GHAHREMANINEZHAD A, DIXON D G, ASSELIN E. Electrochemical and XPS analysis of chalcopyrite ($CuFeS_2$, dissolution in sulfuric acid solution [J]. Electrochimica Acta, 2013, 87: 97−112.

[5] LI Y, QIAN G, LI J, GERSON A R. Kinetics and roles of solution and surface species of chalcopyrite dissolution at 650 mV [J]. Geochimica et Cosmochimica Acta, 2015, 161: 188−202.

[6] RUIZ-SANCHEZ A, LAPIDUS G T. Study of chalcopyrite leaching from a copper concentrate with hydrogen peroxide in aqueous ethylene glycol media [J]. Hydrometallurgy, 2017, 169: 192−200.

[7] MARTINEZ-GOMEZ V J, FUENTES-ACEITUNO J C, PEREZ-GARIBAY R, LEE J. A study of the electro-assisted reductive leaching of a chalcopyrite concentrate in HCl solutions. Part I: Kinetic behavior and nature of the chalcopyrite reduction [J]. Hydrometallurgy, 2018, 181: 195−205.

[8] BARHOUMI N, OLVERA-VARGAS H, OTURAN N, HUGUENOT D, GADRI A, AMMARE S, BRILLAS E, OTURAN M A. Kinetics of oxidative degradation/ mineralization pathways of the antibiotic tetracycline by the novel heterogeneous electro-Fenton process with solid catalyst chalcopyrite [J]. Applied Catalysis B: Environmental, 2017, 209: 637−647.

[9] THURSTON R S, MANDERNACK K W, SHANKS III W C. Laboratory chalcopyrite oxidation by *Acidithiobacillus ferrooxidans*: Oxygen and sulfur isotope fractionation [J]. Chemical Geology, 2010, 269: 252−261.

[10] ZHAO H, HU M, LI Y, ZHU S, QIN W, QIU G, WANG J. Comparison of electrochemical dissolution of chalcopyrite and bornite in acid culture medium [J]. Transactions of Nonferrous Metals Society of China, 2015, 25: 303−313.

[11] ZHAO H, WANG J, QIN W, ZHENG X, TAO L, GAN X, QIU G. Surface species of chalcopyrite during bioleaching by moderately thermophilic bacteria [J]. Transactions of Nonferrous Metals Society of China, 2015, 25: 2725−2733.

[12] WU S, YANG C, QIN W, JIAO F, WANG J, ZHANG Y. Sulfur composition on surface of chalcopyrite during its bioleaching at 50 °C [J]. Transactions of Nonferrous Metals Society of China, 2015, 25: 4110−4118.

[13] LI Y, QIAN G, BROWN P L, GERSON A R. Chalcopyrite dissolution: Scanning photoelectron microscopy examination of the evolution of sulfur species with and without added iron or pyrite [J]. Geochimica et Cosmochimica Acta, 2017, 212: 33−47.

[14] CHIRITA P, SCHLEGEL M L. Oxidative dissolution of iron monosulfide (FeS) in acidic conditions: The effect of solid pretreatment [J]. International Journal of Mineral Processing, 2015, 135: 57−64.

[15] LINGE H G. A study of chalcopyrite dissolution in acidic ferric nitrate by potentiometric titration [J]. Hydrometallurgy, 1976, 2: 51−64.

[16] DUTRIZAC J E. The kinetics of dissolution of chalcopyrite in ferric ion media [J]. Metallurgical and Materials Transactions B, 1978, 9: 431−439.

[17] BASOLO F, PEARSON R G. Mechanisms of Inorganic Reactions. A study of metal complexes in solution [M]. 2nd Edition. New York: John Wiley and Sons, Inc, 1967.

[18] SCHOONEN M A A, STRONGIN D R. Catalysis of electron transfer reactions at mineral surfaces [M]. Environmental Catalysis. GRASSIAN V H ed.. Boca Raton, Fl: CRC Press, 2005.

[19] SHU X, DANG Z, ZHANG Q, YI X, LU G, GUO C, YANG C. Passivation of metal-sulfide tailings by covalent coating [J]. Minerals Engineering, 2013, 42: 36−42.

[20] CHIRITA P, DUINEA M I, SANDU A M, BIRSA L M, SARBU L G, BAIBARAC M, SAVA F, POPESCU M, MATEI E. Inhibitory effect of three phenacyl derivatives on the oxidation of sphalerite (ZnS) in air-equilibrated acidic solution [J]. Corrosion Science, 2018, 138: 154−162.

[21] BADICA C E, CHIRITA P. An electrochemical study of the oxidative dissolution of iron monosulfide (FeS) in air-equilibrated solutions [J]. Electrochimica Acta, 2015, 178: 786−796.

[22] BABIC-SAMARDZIJA K, KHALED K F, HACKERMAN N. Investigation of the inhibiting action of O^-, S^- and N-dithiocarbamato(1,4,8,11-tetraazacyclotetradecane) cobalt (III) complexes on the corrosion of iron in HClO4 acid [J]. Applied Surface Science, 2005, 240: 327−340.

[23] ABDALLAH Y M. Electrochemical studies of phenyl sulphonyl ethanone derivatives compounds on corrosion of aluminum in 0.5 M H_2SO_4 solutions [J]. Journal of Molecular Liquids, 2016, 219: 709−719.

[24] EL BELGHITI M, KARZAZI Y, DAFALI A, HAMMOUTI B, BENTISS F, OBOT I B, BAHADUR I, EBENSO E E. Experimental, quantum chemical and Monte Carlo simulation studies of 3,5-disubstituted-4-amino-1,2,4-triazoles as corrosion inhibitors on mild steel in acidic medium [J]. Journal of Molecular Liquids, 2016, 218: 281−293.

[25] GECE G, BILGIC S. Quantum chemical study of some cyclic nitrogen compounds as corrosion inhibitors of steel in NaCl media [J]. Corrosion Science, 2009, 51: 1876−1878.

[26] QIANG Y, ZHANG S, XU S, LI W. Experimental and theoretical studies on the corrosion inhibition of copper by two indazole derivatives in 3.0% NaCl solution [J]. Journal of Colloid and Interface Science, 2016, 472: 52−59.

[27] KOLEINI S M J, AGHAZADEH V, SANDSTROM A. Acidic sulphate leaching of chalcopyrite concentrates in presence of pyrite [J]. Minerals Engineering, 2011, 24: 381−386.

[28] MANESCU S, CUCU M, DIACONESCU M L. Environmental sanitary chemistry [M]. Bucharest: Medical

Publishing House, 1994. (in Romanian)

[29] TE VELDE G, BAERENDS E J. Precise density-functional method for periodic structures [J]. Physical Review B, 1991, 44: 7888−7903.

[30] ADF manual, ADF modeling suite 2016 [M]. 2016. http://www.scm. com.

[31] van LENTHE E, BAERENDS E J, SNIJDERS J G. Relativistic regular two-component Hamiltonians [J]. The Journal of Chemical Physics, 1993, 99: 4597−4610.

[32] ROSA A, BAERENDS E J, van GISBERGEN S J, LENTHE A E, GROENEVELD J A, SNIJDERS J G. Electronic spectra of M(CO)6 (M=Cr, Mo, W) revisited by a relativistic TDDFT approach [J]. Journal of the American Chemical Society, 1999, 121: 10356−10365.

[33] HOU M, MEI Q, HAN B. Solvent effects on geometrical structures and electronic properties of metal Au, Ag, and Cu nanoparticles of different sizes [J]. Journal of Colloid Interface Science, 2015, 449: 488−493.

[34] VOSKO S H, WILK L, NUSAIR M. Accurate spin-dependent electron liquid correlation energies for local spin density calculations: A critical analysis [J]. Canadian Journal of Physics, 1980, 58: 1200−1211.

[35] PERDEW J P, CHEVARY J A, VOSKO S H, JACKSON K. A, PEDERSON M R, SING D J, FIOLHAIS C. Atoms, molecules, solids, and surfaces: Applications of the generalized gradient approximation for exchange and correlation [J]. Physical Review B, 1992, 46: 6671−6687.

[36] CONSTANTIN C A, CHIRITA P. Oxidative dissolution of pyrite in acidic media [J]. Journal of Applied Electrochemistry, 2013, 43: 659−666.

[37] CHIRITA P, SCHLEGEL M L. Pyrite oxidation in air-equilibrated solutions: An electrochemical study [J]. Chemical Geology, 2017, 470: 67−74.

[38] TUKEN T, YAZICI B, ERBIL M. The corrosion behaviour of polypyrrole coating synthesized in phenylphosphonic acid solution [J]. Applied Surface Science, 2006, 252: 2311−2318.

[39] DESCOSTES M, BEAUCAIRE C, MERCIER F, SAVOYE S, SOW J, ZUDDAS P. Effect of carbonate ions on pyrite (FeS_2) dissolution [J]. Bulletin of the Geological Society of France, 2002, 173: 265−270. (in French)

[40] MIKHLIN Y L, KUKLINSKIY A V, PAVLENKO N I, VARNEK V A, ASANOV I P, OKOTRUB A V, SELYUTIN G E, SOLOVYEV L A. Spectroscopic and XRD studies of the air degradation of acid-reacted pyrrhotites [J]. Geochimica et Cosmochimica Acta, 2002, 66: 4057−4067.

[41] PENG T, ZHOU D, LIU X, YU R, JIANG T, GU G, CHEN M, QIU G, ZENG W. Enrichment of ferric iron on mineral surface during bioleaching of chalcopyrite [J]. Transactions of Nonferrous Metals Society of China, 2016, 26: 544−550.

[42] CHANG K, ZHANG Y, ZHANG J, LI T, WANG J, QIN W. Effect of temperature-induced phase transitions on bioleaching of chalcopyrite[J]. Transactions of Nonferrous Metals Society of China, 2019, 29: 2183−2191.

[43] CHIRITA P, DESCOSTES M. Troilite oxidation by hydrogen peroxide [J]. Journal of Colloid and Interface Science, 2006, 299: 260−269.

[44] CHIRITA P. Aqueous oxidation of iron monosulfide (FeS) by molecular oxygen [J]. Mineral Processing and Extractive Metallurgy Review, 2016, 37: 305−310.

[45] CHIRITA P. Evaluation and modeling of the surface characteristics of troilite (FeS) [J]. Applied Surface Science, 2019, 480: 281−287.

[46] YANG B, LUO W, LIAO Q, ZHU J, GAN M, LIU X, QIU G. Photogenerated-hole scavenger for enhancing photocatalytic chalcopyrite bioleaching [J]. Transactions of Nonferrous Metals Society of China, 2020, 30: 200−211.

[47] BAMPOLE D L, LUIS P, MULABA-BAFUBIANDI A F. Sustainable copper extraction from mixed chalcopyrite-chalcocite using biomass [J]. Transactions of Nonferrous Metals Society of China, 2019 29: 2170−2182.

[48] TAO D P, RICHARDSON P E, LUTTRELL G H, YOON R H. Electrochemical studies of pyrite oxidation and reduction using freshly-fractured electrodes and rotating ring-disc electrodes [J]. Electrochimica Acta, 2003, 48: 3615−3623.

[49] XI S, ZHANG X, LUAN Z, DU Z, LI L., LIANG Z, LIAN C, YAN J. Micro-Raman study of thermal transformations of sulfide and oxysalt minerals based on the heat induced by laser [J]. Minerals, 2019, 9(12): 751.

[50] WANG C, XUE S, HU J, TANG K. Raman, far infrared, and Mossbauer spectroscopy of CuFeS2 nanocrystallites [J]. Japanese Journal of Applied Physics, 2009, 48: 023003.

[51] PRAMEENA B, ANBALAGAN G, GUNASEKARAN S, RAMKUMAAR G R, GOWTHAM B. Structural, optical, electron paramagnetic, thermal and dielectric characterization of chalcopyrite [J]. Spectrochimica Acta (Part A): Molecular and Biomolecular Spectroscopy, 2014, 122: 348−355.

[52] LIANG C, XIA J, NIE Z, YU S, XU B. Effect of initial pH on chalcopyrite oxidation dissolution in the presence of extreme thermophile *Acidianus manzaensis* [J]. Transactions of Nonferrous Metals Society of China, 2014, 24: 1890−1897.

[53] FITOZ A, NAZIR H, OZGUR (nee YAKUT) M, EMREGUL E, EMREGUL K C. An experimental and theoretical approach towards understanding the inhibitive behavior of a nitrile substituted coumarin compound as an effective acidic media inhibitor [J]. Corrosion Science, 2018, 133: 451−464.

[54] HU K, ZHUANG J, DING J, MA Z, WANG F, ZENG X. Influence of biomacromolecule DNA corrosion inhibitor on carbon steel [J]. Corrosion Science, 2017, 125: 68−76.

[55] BEDAIR M A, EL-SABBAH M M B, FOUDA A S, ELARYIAN H M. Synthesis, electrochemical and quantum chemical studies of some prepared surfactants based on azodye and Schiff base as corrosion inhibitors for steel in acid medium [J]. Corrosion Science, 2017, 128: 54−72.

黄铜矿在空气平衡的酸性溶液中的氧化：苯酰基衍生物的抑制作用

Paul CHIRIȚĂ[1], Mădălina I. DUINEA[1,2], Laura G. SÂRBU[3],
Lucian M. BÎRSĂ[3], Mihaela BAIBARAC[4], Florinel SAVA[4], Elena MATEI[4]

1. Department of Chemistry, University of Craiova, Calea Bucuresti 107I, 200478, Craiova, Romania;
2. Department of Chemistry, Physics and Environment,
"Dunarea de Jos" University of Galati, 111 Domneasca Street, Galati 800201, Romania;
3. Department of Chemistry, "Al. I. Cuza" University of Iasi, 11 Carol I Blv., Iasi 700506, Romania;
4. Lab. Optical Processes in Nanostructured Materials, National Institute of Materials Physics,
P. O. Box MG-7, Bucharest, R077125, Romania

摘　要：研究 4-(2-羟苯基)-2-(-4-吗啉基)-1,3-噻唑（Pr02）、1-(3,5-二溴-2-羟苯基)-1-(2-氧乙基)-*N*,*N*-二乙基二硫代氨基甲酸酯(Pr04)和 1-(5-溴-2-羟基-3-甲苯基)-1-(2-氧乙基)-*O*-乙基黄原酸酯(Pr06)对黄铜矿($CuFeS_2$)在温度 25 °C、pH 2.5 的空气平衡溶液中液相氧化反应的影响。采用动电位极化、电化学阻抗谱(EIS)、能谱扫描电镜(SEM/EDX)分析、液相间歇实验、傅里叶变换红外光谱(FTIR)、拉曼散射以及量子化学计算等方法研究这些影响，发现阳极电流密度按 EtOH> Pr02> Pr04> Pr06 的顺序降低。这些结果以及 EIS 测量结果表明，Pr02、Pr04 和 Pr06 是黄铜矿液相氧化的有效阳极抑制剂。拉曼散射和 FTIR 光谱分析表明，矿物表面形成的元素硫、多硫化物和羟基氧化铁与黄铜矿的液相氧化抑制作用无关。量子化学计算表明，所测试的化合物在黄铜矿表面的吸附在能量上是有利的，从而可以解释所观察到的这些化合物的抑制作用。

关键词：黄铜矿氧化；苯酰基衍生物；抑制；动电位极化；量子化学计算

(Edited by Xiang-qun LI)